Walfre Franco
Ph.D.
Beckman Laser Institute,
University of California,
Irvine, CA 92612;
Department of Mechanical Engineering,
University of California,
Riverside, CA 92521
e-mail: wfranco@uci.edu

Henry Vu
B.S.
Department of Mechanical Engineering,
University of California,
Riverside, CA 92521

Wangcun Jia
Ph.D.

J. Stuart Nelson
M.D., Ph.D.

Beckman Laser Institute,
University of California,
Irvine, CA 92612

Guillermo Aguilar
Ph.D.
Department of Mechanical Engineering,
University of California,
Riverside, CA 92521

Fluid and Thermal Dynamics of Cryogen Sprays Impinging on a Human Tissue Phantom

Cryogen spray cooling (CSC) protects the epidermis from unintended heating during cutaneous laser surgery. The present work investigated the time-dependent flow characteristics of cryogen sprays and correspondent thermal dynamics at the surface of a human tissue phantom. First, a numerical analysis was carried out to evaluate an epoxy block substrate as a human tissue phantom. Next, the velocity and diameter of cryogen droplets were measured simultaneously and correlated with surface temperature of the human tissue phantom during CSC. Finally, velocity and diameter measurements were used to compute the spray number, mass, and kinetic energy fluxes, and temperature measurements were used to compute the surface heat flux. Numerical modeling showed that the thermal response of our phantom was qualitatively similar to that of human stratum corneum and epidermis; quantitatively, thermal responses differed. A simple transformation to map the temperature response of the phantom to that of tissue was derived. Despite the relatively short spurt durations (10 ms, 30 ms, and 50 ms), cryogen delivery is mostly a steady state process with initial and final fluid transients mainly due to the valve dynamics. Thermal transients (16 ms) are longer than fluid transients (4 ms) due to the low thermal diffusivity of human tissues; steady states are comparable in duration ($\approx$10 ms, 30 ms, and 50 ms) although there is an inherent thermal delay ($\approx$12 ms). Steady state temperatures are the lowest surface temperatures experienced by the substrate, independent of spurt duration; hence, longer spurt durations result in larger exposures of the tissue surface to the same lower, steady state temperature as in shorter spurts. Temperatures in human tissue during CSC for the spray system and parameters used herein are estimated to be $\approx -19\,^{\circ}C$ at the stratum corneum surface and $>0\,^{\circ}C$ across the epidermis. [DOI: 10.1115/1.2948404]

1 Introduction

Cryogen spray cooling (CSC) has proven essential for successful cutaneous laser surgery without adverse effects. A short cryogen spurt precools the epidermis during laser irradiation to avoid unintended injury therein from excessive heating induced by melanin absorption [1,2]. Heat extraction from tissue during CSC is a function of many fundamental spray parameters, such as average droplet velocity and diameter, mass flow rate, temperature, and spray density [3–7], that vary in time and space within the spray cone. There are many experimental and numerical studies that describe the thermal dynamics imposed by CSC on tissue models. However, only a few studies considered the spray characteristic structure in steady state, namely, droplet velocity and diameter distributions. Karapetian et al. [4] reported droplet velocity and diameter ranges of 28–72 m/s and 12–18 μm, respectively, for inner nozzle diameters of 0.57–1.33 mm and two lengths of 8 mm and 65 mm. It was concluded that changes in mass flow rate have a larger effect on the surface heat flux than changes in droplet size, and that for fully atomized sprays changes in velocity can substantially impact the surface heat flux. Pikkula et al. [5] reported that sprays with a higher Weber number (ratio of inertial forces to surface tension) increase heat removal; i.e., higher velocities and larger droplets enhance surface heat transfer. Hsieh and Tsai [8] also studied the effect of spray characteristics and mass flow on the surface heat flux using small nozzle diameters, 0.2–0.4 mm, at different nozzle-substrate distances. The authors proposed that nozzles with smaller diameters than those in current use may enhance surface cooling. While these experimental studies describe the thermal dynamics imposed by CSC on tissue models, they all consider the spray characteristic structure in steady state only. To the best of our knowledge, this is the first study correlating spray droplet dynamics (average velocity and diameter) and surface thermal dynamics (temperature and heat flux) during CSC of human tissue. A better understanding of CSC dynamics is essential for optimizing laser procedures, improving current technologies and providing insights into biophysical responses. For example, different studies have investigated multiple-intermittent cryogen spurts and laser pulses to improve cutaneous laser surgery [9–11]. Characterization of the spray system dynamics is fundamental to develop this technology. It is important to acknowledge the significant work of a large community devoted to liquid atomization and sprays, where related problems have been addressed and some of the analytical tools used herein have been developed. The main differences between previous work and our intended application to human tissue are the low thermal diffusivity of the substrate and the short spurt durations.

2 Objectives

The objectives of the present study are (i) to evaluate an epoxy block substrate as a thermal model of human tissues, namely, stratum corneum and epidermis, (ii) determine the flow characteristics of cryogen sprays in steady and transient states impinging onto the human tissue phantom, (iii) correlate the spray character-

Contributed by the Bioengineering Division of ASME for publication in the JOURNAL OF BIOMECHANICAL ENGINEERING. Manuscript received July 20, 2007; final manuscript received April 16, 2008; published online July 11, 2008. Review conducted by John C. Bischof. Paper presented at the 2007 ASME-JSME Thermal Engineering Conference and Summer Heat Transfer Conference (HT2007), Vancouver, British Columbia, Canada, July 8–12, 2007.

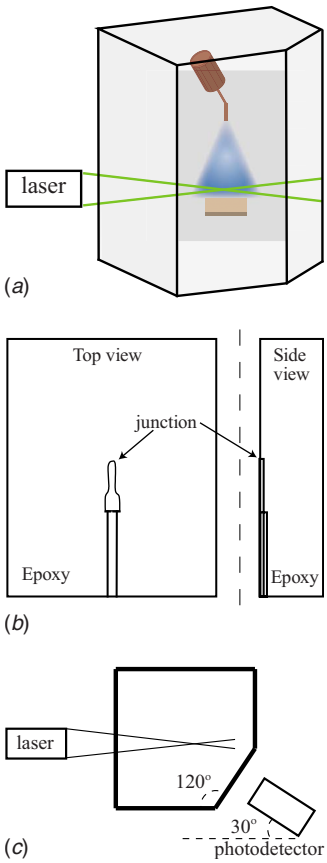

Fig. 1 Schematic of tight-seal acrylic chamber, spray system, tissue phantom, and PDPA components. (*a*) Spray system and tissue phantom were placed inside to conduct experiments at reduced, constant relative humidity levels (16–18%). (*b*) A thin film thermocouple embedded in epoxy was used to measure surface temperatures. (*c*) Chamber walls were designed to be perpendicular to PDPA components to minimize refraction.

istics to the surface heat transferred from the human tissue phantom, and (iv) provide an estimate of the temperatures to be expected in human skin. Spray transient state refers to the period when average droplet velocity and diameter vary over time. The initial and final transients occur when the spray valve opens and closes, respectively.

3 Experimental and Numerical Methods

3.1 Spray System. Refrigerant hydrofluorocarbon 134a (Suva® 134a, Dupont) was delivered through a high pressure hose to an electronic valve (Series 99, Parker Hannifin Corp., Cleveland, OH) attached to an angled-tube nozzle (120 deg) with a length and inner diameter of 40 mm and ≈0.5 mm, respectively. The valve and nozzle were from a commercial skin cooling device (GentleLase, Candela, Wayland, MA). The spray system was set to deliver a downward vertical spray. R134a (boiling temperature at atmospheric pressure ≈−26°C) was kept in its original container at 600 kPa and 21°C. Spurt durations of 10 ms, 30 ms, and 50 ms were investigated. A schematic of the spray system is shown in Fig. 1(*a*).

3.2 Phase Doppler Anemometry and Particle Sizing. Spray droplet velocity and diameter were measured with a phase Doppler particle analyzer (PDPA, TSI Incorporated, Shoreview, MN). Although this system was capable of measuring velocity along the two perpendicular axes, only axial velocities were considered because measurements correspond to the cone center of vertical cryogen sprays. The nozzle-to-phantom distance was 35 mm and the PDPA measurement volume was set 2.5 mm above the human tissue phantom; i.e., 32.5 mm away from the nozzle tip. For the analysis of droplet dynamics, velocity and diameter measurements were split in 1 ms time windows. Approximately ten experiments were conducted for each spurt duration under study to obtain a minimum of 100 data points in each time bin. The deviation percentage from the cumulative size distribution as a function of the sample size M can be estimated as $127.32M^{-0.49212}$, which corresponds to a maximum deviation of 13% in our study [12].

Table 1 Thermal properties of tissue with 0.2 g and 0.6 g of water/g of total tissue [20] and epoxy [25]

	Tissue (0.3 water content)	Tissue (0.6 water content)	Epoxy
k (W/m K)	0.13	0.34	0.14
ρ (kg/m^3)	1210	1120	1019
c (J/kg K)	2241	3200	1631
α (m^2/s)	4.7×10^{-8}	9.5×10^{-8}	8.4×10^{-8}

3.3 Human Tissue Phantom and Thermal Sensor. The human tissue phantom and thermal sensor consisted of an epoxy resin (EP30-3, Master Bond, Inc., Hackensack, NJ) with a thin-foil thermocouple (CO2-K, Omega Engineering, Stamford, CT) embedded at the surface, as shown schematically in Fig. 1(*b*). Although the width and length of the thermocouple measurement junction are ≈0.5 mm, the thin-foil sensor has a thickness of 13 μm to provide high vertical temperature resolution. This feature makes the sensor suitable for measuring surface temperature during CSC because the vertical temperature gradient in either a tissue phantom or human skin is much greater than that in the lateral direction [6]. The estimated response time is 2 ms and measurement uncertainty associated with K-type thermocouples is 0.28°C after calibration. Thermal properties of tissues with different water contents and epoxies are shown in Table 1. Details about preparation of the tissue phantom can be found in Ref. [13]. The measurement junction was aligned with the center of the spray cone, where the highest heat extraction occurs, and the tissue phantom was placed 35 mm away from the nozzle tip. Since PDPA and temperature measurements were performed simultaneously, Sec. 4 presents the average temperature measurements of approximately ten experiments.

3.4 Isolation Chamber. The spray system and tissue phantom were placed inside a custom made chamber to maintain a reduced, constant relative humidity level, which is known to affect the efficiency of heat extraction from the tissue [14,15] and experimental repeatability. The chamber, schematically shown in Figs. 1(*a*) and 1(*c*), is made of transparent acrylic walls 12.7 mm thick. The walls were designed to be perpendicular to the PDPA's transmitter (laser beams) and receiver (photodetector) to minimize refraction and did not have an effect on droplet velocity although droplet diameter decreased (1–2 μm). Relative humidity levels were kept at 16–18% by flushing the chamber with dry air.

3.5 Spray Flux Calculations. Droplet velocity and size are two of the primary measurements required to calculate spray fluxes. The velocity is not likely to influence the overall flux or concentration accuracy, since it is commonly measured with high accuracy. However, flux calculations are very sensitive to inaccuracies in droplet size measurements, which are elevated to the second or third power to calculate surface area or volume flux. Significant size errors can be made when the signal-to-noise ratio is low or if the assumption that a single scattering mode is dominant no longer holds. Rejection of improperly sized droplets or size validation has the disadvantage that these droplets are then missing in subsequent flux calculations. This then leads to a third primary measurement quantity, the number of particles passing

through the detection volume during a given observation time. In addition to rejection due to the size validation, sources for counting errors are small droplets that fall below the detection threshold of the system and multiple particle passing simultaneously through the detection volume, leading to particle rejection or erroneous size information.

In this study, we used a model that accounts for the complex geometry of the detection volume and for the probability of two or more drops in the probe volume simultaneously. The model is based on the assumption that the drops in the spray are distributed randomly and, consequently, the probability of two or more drops in the probe volume can be derived using the Poisson distribution. It is well known that for relatively dense sprays, such as cryogen sprays at a short distance from the nozzle, the influence of overlapping signals from two or more drops on flux calculations may be significant [16].

The number, mass, and kinetic energy fluxes of cryogen sprays were estimated from PDPA measurements following [16]

$$\varphi = \frac{1}{\tau}\sum_{i=1}^{N} \frac{\eta_i \varphi_i}{A_{\gamma,i}(D_i,\gamma_i)} \vec{e}_{\gamma,i} \tag{1}$$

where

$$\varphi_i = \begin{cases} 1 & \text{for the number flux} \\ \dfrac{\pi\rho}{6} D_i^3 & \text{for the mass flux} \\ \dfrac{\pi\rho}{12} D_i^3 V_i^2 & \text{for the kinetic energy flux} \end{cases} \tag{2}$$

τ is the measurement time, N is the number of validated signals, η is a correction factor, A_γ is the reference area of the detection volume, D is the diameter of the ith droplet, γ is the particle trajectory angle, $\vec{e}_\gamma$ is the unit vector in the direction of the droplet motion, ρ is the density, and V is the droplet velocity. In addition to D and γ, A_γ is also a function of V, burst duration, and hardware parameters (such as the width of the projected slit and the receiver off-axis angle). η accounts for count errors due to multiple particle scattering or for nonvalidation of particles and is a function of the relative signal presence (in the measured volume) of the validated and nonvalidated signals. We used the coincident mode of our PDPA system to define validated signals; within this operational mode, a droplet diameter measurement corresponds to a simultaneous velocity measurement. With the coincident mode off, every signal corresponds to a velocity measurement but not necessarily to a diameter measurement. Coincident and noncoincident measurements counts per 1 ms bin are shown for 10 ms, 30 ms, and 50 ms spurts in Fig. 2. Except for the last two bins in each figure (which are excluded from computations), there are more than 100 samples per bin. The difference between the noncoincident and coincident measurement counts represents the number of nonvalidated particle size measurements, which in our PDPA system correspond to mismatches between two independent phase shift (particle size) measurements; the system only accepts the velocity measurement. This situation may arise, for example, when there are two or more drops in the probe volume simultaneously. For details about the computation of η and A_γ, the reader is referred to Ref. [16].

3.6 Heat Flux Calculations. Temperatures recorded by the thin-foil sensor were assumed to be surface temperatures because the foil Biot number (hL/k) for a heat transfer coefficient $h = 20{,}000\ \mathrm{W/m^2\,K}$ [17], characteristic length $L = 13\times10^{-6}$ m, and thermal conductivity $k = 12\ \mathrm{W/m\,K}$ [18] is $\approx 2\times10^{-2}$; i.e., the temperature of the foil is spatially uniform, $hL/k \leq 1$. The following analytical expression based on Fourier's law and Duhamel's theorem was used to compute the surface heat flux q'' from the experimental temperature T:

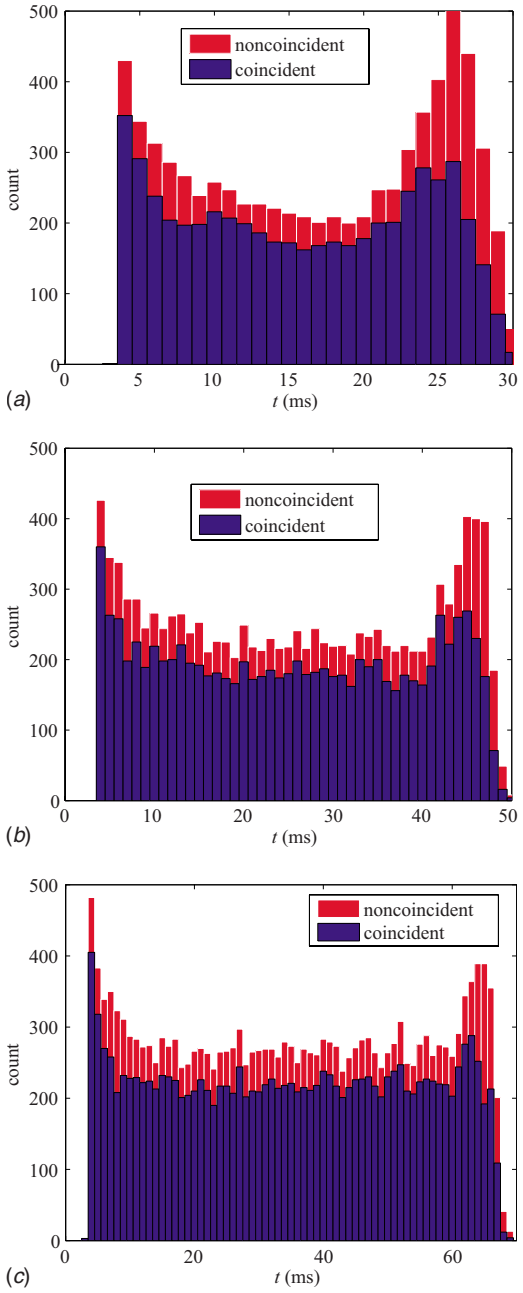

Fig. 2 Count of coincident and noncoincident measurements in 1 ms time bins during CSC

$$q''_J = 2\sqrt{\frac{k\rho c}{\pi}} \sum_{j=1}^{J} \frac{T_j - T_{j-1}}{\sqrt{t_J - t_j} + \sqrt{t_J - t_{j-1}}} \tag{3}$$

where J is the total number of temperature measurements, ρ is the density, c is the specific heat, and t is the time. A detailed derivation of Eq. (3) can be found in Refs. [6,19].

3.7 Heat Transfer Modeling. To model the thermal response of human tissue and epoxy to CSC, we solved the two-dimensional heat conduction equation:

$$\rho c \frac{\partial}{\partial t}\theta(x,y,t) - \nabla(k \nabla\, \theta(x,y,t)) = 0 \tag{4}$$

for which the surface boundary condition was specified as

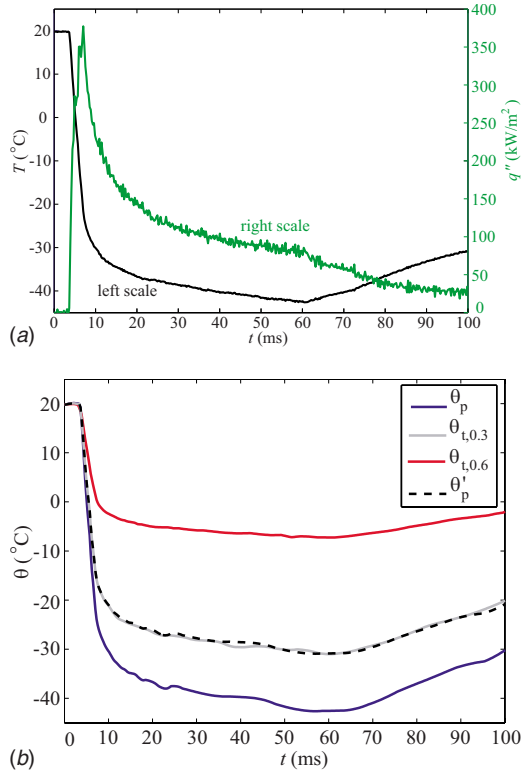

Fig. 3 (*a*) Experimental surface temperature (left scale) and estimated surface heat flux q'' (right scale). (*b*) Tissue and phantom surface temperature response, θ_t and θ_p, to q'', and mapped temperature, θ'_p, matching tissue response.

$$-k\nabla\theta(x,0,t)\cdot\vec{n}=q''(t) \tag{5}$$

where θ is the numerical substrate temperature, x and y are, respectively, the lateral and vertical coordinates, $\vec{n}$ is the unit vector normal to the surface, and q'' is the surface heat extraction computed from experimental measurements using Eq. (3). At the other boundaries $-k\nabla\theta\cdot\vec{n}=0$. The computation domain was the following: -1×10^{-3} m$\leq x\leq 1\times10^{-3}$ m, -1.5×10^{-3} m$\leq y\leq 0$ m. Tissue thermal properties were approximated with empirical relations [20] and measured water content [21], Table 1. Thermal responses were modeled for human tissues with 0.3 g and 0.6 g of water/g of total tissue, which correspond to the water content in the stratum corneum and epidermis, respectively.

4 Results and Analysis

4.1 Epoxy Substrate as a Human Tissue Phantom. Figure 3(*a*) shows the experimental surface temperature T (left scale) during a 50 ms CSC spurt onto the tissue phantom and the corresponding surface heat flux q'' (right scale). This heat flux is next used as the boundary condition for comparing the thermal response between human tissues and tissue phantom. Figure 3(*b*) shows the numerical surface temperatures of the tissue with 0.3 and 0.6 water content, $\theta_{t,0.3}$ and $\theta_{t,0.6}$, and phantom, θ_p. The greatest temperature drops in tissues and phantom are $\Delta\theta_{t,0.3}=51°$C, $\Delta\theta_{t,0.6}=27°$C, and $\Delta\theta_p=63°$C, respectively; temperature drops are 91%, 92%, and 93% of $\Delta\theta_{t,0.3}$, $\Delta\theta_{t,0.6}$, and $\Delta\theta_p$, respectively, at $t=20$ ms; lowest surface temperatures, $-31°$C, $-7°$C, and $-43°$C, occur at $t\approx60$ ms, 61 ms, and 57 ms, respectively. Although dynamic responses of tissues and phantom to the same time-dependent heat flux are qualitatively similar, θ_p is considerably lower than θ_t. This is not surprising because the density—and mass for the same volume—and ability to conduct heat of these materials are comparable; however, more heat is needed to change the temperature of the tissues as compared to the epoxy, Table 1.

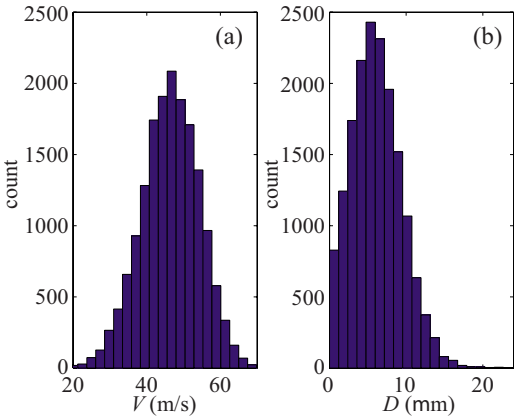

Fig. 4 (*a*) Velocity and (*b*) diameter distributions for the cone center of a cryogen spray in steady state 32.5 mm away from the nozzle tip

It is possible to introduce a simple transformation to map θ_p to θ_t as follows:

$$\theta'_p(t)=\theta_o+\xi(\theta_p(t)-\theta_o) \tag{6}$$

where θ_o is the initial temperature of the phantom and

$$\xi=\frac{k_p\sqrt{\alpha_t}}{k_t\sqrt{\alpha_p}} \tag{7}$$

The transformation is based on the analytical solution for constant surface heat flux evaluated at the surface [18]. Mapping of the epoxy surface temperature response to that of tissue with 0.3 water content, $\theta'_{p,0.3}$, is shown in Fig. 3(*b*), $\theta'_{p,0.3}=\theta_{t,0.3}$. Our results show that, assuming heat transferred from an epoxy tissue phantom during CSC is the same as that from tissue, $\Delta\theta_{t,0.3}$ and $\Delta\theta_{t,0.6}$ are $\approx$81% and 43% of $\Delta\theta_p$, respectively. Therefore, the thermal response of epoxy is better suited to study low-water content tissues, such as the stratum corneum, despite having a thermal diffusivity closer to that of the epidermis. However, the problem is far more complex as q'' is a function of the substrate thermal properties and spray thermodynamics such as phase (liquid and vapor) and temperatures. Dynamics of q'' during CSC of human tissue may be similar to those reported in this study; however, q'' might be quantitatively smaller and, subsequently, θ_t may drop even less than shown in Fig. 3(*b*).

We assumed that CSC would induce the same $q''(t)$ on each substrate and computed $\theta(t)$ to be able to compare dynamic thermal responses. An alternative approach would be to assume that CSC induces the same $\theta(t)$ on each substrate and compute $q''(t)$. To satisfy $\theta(t)_{s,0.6}=\theta(t)_{s,0.3}=\theta(t)_p$, it follows that $q''(t)_{s,0.6}>q''(t)_{s,0.3}>q''(t)_p$ because more heat extraction is needed to lower the temperature of substrates with higher specific heat, as stated above.

4.2 Spray Characteristics in Steady State. Figure 4 shows steady state velocity and diameter distributions for a 50 ms cryogen spurt at the cone center and 32.5 mm away from the nozzle tip. The total droplet count was 16,660, which resulted in a 1.1% deviation from the cumulative size distribution. Figure 4 shows that for a commercial spray system the velocities of cryogen droplets impinging onto the tissue surface range from 20 m/s to 70 m/s and average of 48 m/s. Droplet diameters as large as 15 μm and 6 μm on average were measured inside the chamber. However, because the chamber effects droplet diameter, droplets are expected to be as large as 17 μm and on average 8 μm under atmospheric conditions at the laboratory or clinic. Experiments at different relative humidity levels (16–50%) re-

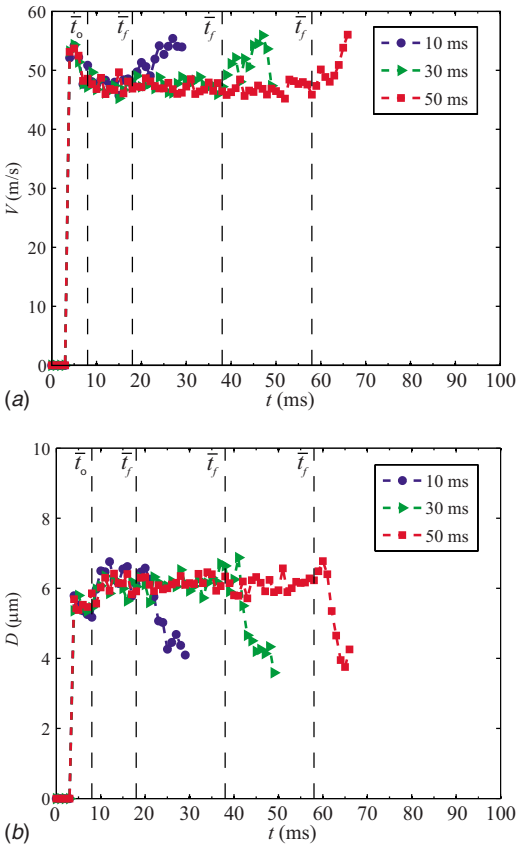

Fig. 5 Average cryogen droplet (*a*) velocity and (*b*) diameter as a function of time during 10 ms, 30 ms, and 50 ms cryogen spurts. The vertical dashed lines represent the beginning and end, $\bar{t}_o$ and $\bar{t}_f$, of the spray steady state.

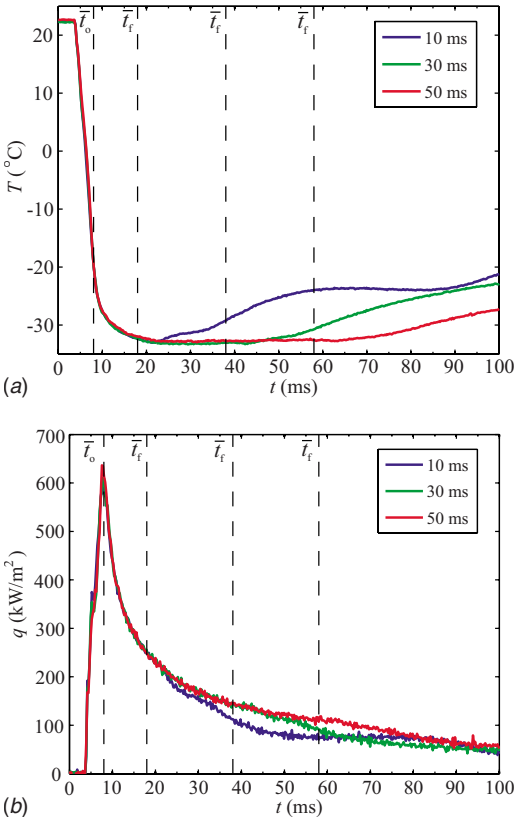

Fig. 6 Average tissue phantom surface (*a*) temperature and (*b*) heat flux as a function of time during 10 ms, 30 ms, and 50 ms spurts. The vertical dashed lines represent the beginning and end, $\bar{t}_o$ and $\bar{t}_f$, of the spray steady state.

sulted in the same velocity and diameter values and distributions; i.e., the spray characteristics were not sensitive to changes in relative humidity conditions. Average velocity and diameter are in agreement with those reported in Ref. [4], 40 m/s and 13 mm, for a 25 mm nozzle-surface distance and a similar nozzle (65 mm length, 0.57 mm inner diameter). Although average droplet velocity and size for CSC of human tissue have been measured before [22], Fig. 4 shows the velocity and size distribution for a spray system and parameters currently used in clinical practice.

4.3 Fluid and Heat Transfer Dynamics During CSC

4.3.1 Spray Fluid Dynamics. Average droplet velocity V and diameter D as a function of time during 10 ms, 30 ms, and 50 ms spurts are shown in Fig. 5. The times at which the steady states began, $\bar{t}_o$, and ended, $\bar{t}_f$, are represented by vertical dashed lines. Cryogen droplets took $\approx$4 ms to reach the tissue phantom surface after the valve was energized. Independent measurements of laser light transmittance at the nozzle exit (not included) showed that this initial delay was mainly due to the valve's opening mechanics. Furthermore, if the initial droplets $V>50$ ms, their in-flight time from the nozzle to the phantom surface would be <0.7 ms, which is only a small fraction of the total delay time. For each spurt, the initial and final spray transients, respectively, lasted $\approx$4 ms and 10 ms; these are the times required for the valve to fully open and close, respectively. Figure 5(*a*) shows that during the initial transient, $t=4-8$ ms, V increased reaching a maximum of 55 m/s, then decreased to reach a steady state value $\bar{V}=48$ m/s. During the final transient, V increased monotonically beyond its initial transient maximum value. Final transients began 8 ms after the end of the period in which the normally closed valve was energized (i.e., nominal spurt duration)—these times were also the end of the steady state, represented by vertical dashed lines $\bar{t}_f$ in the figures. Figure 5(*b*) shows that during the transient states, D decreased and increased when V increased and decreased, respectively; i.e., small droplets traveled faster than larger droplets and vice versa. Steady state value $\bar{D}=6$ μm. Flow through an orifice is proportional to the orifice area and fluid velocity; hence, for a constant flow, the velocity is inversely proportional to the orifice area. During valve opening, initial droplets coming from a small orifice traveled faster than those coming from a fully open valve. Initial droplets were also smaller because they comprised the front of the spray and, consequently, were exposed to different surrounding conditions and aerodynamic forces (most likely resulting in different evaporation rates), such as temperature differentials, saturated vapor levels, and drag forces. During valve closure, droplet velocity also increased due to the reductions in orifice area and droplet size decreased due to the changes in aerodynamic forces.

4.3.2 Surface Heat Transfer Dynamics. The average tissue phantom surface temperature T and heat flux q'' as a function of time during 10 ms, 30 ms, and 50 ms spurts are shown in Fig. 6. The vertical dashed lines represent the spray $\bar{t}_o$ and $\bar{t}_f$, which are included to facilitate the transient-state correlation between spray characteristics and phantom cooling. As for the spray fluid dynamics, the initial and final temperature transients can be identified in Fig. 6(*a*). Initially, T decreased abruptly during the first 6 ms ($t=4-10$ ms), continued decreasing at a slower rate during the next 10 ms ($t=10-20$ ms) and, finally, reached steady state $\bar{T}=-33$°C, which was also the lowest surface temperature T_l. During the final transient, T slowly increased to reach room tem-

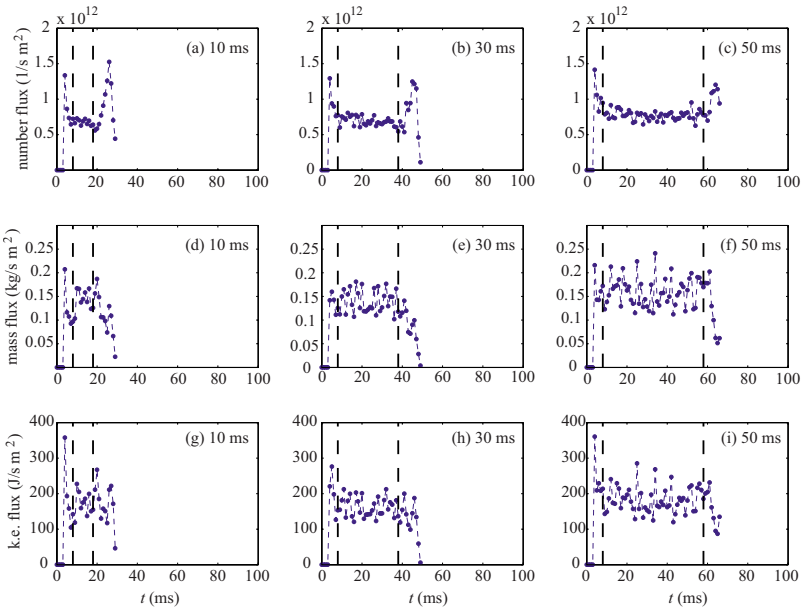

Fig. 7 Spray number, (*a*)–(*c*), mass, (*d*)–(*f*), and kinetic energy, (*g*)–(*i*), fluxes during 10 ms, 30 ms, and 50 ms spurts. The vertical dashed lines represent the beginning and end (left and right lines, respectively) of the spray steady state.

perature. Figure 6(*b*) shows that q'' is highly dynamic: q'' increased abruptly reaching a maximum 5 ms after the droplets impinged on the surface; subsequently, q'' decreased at different rates from high to low—as evidenced by slope changes in the curves. The highest heat flux q''_h=591 kW/m^2 (t=8.1 ms), 611 kW/m^2 (7.8 ms), and 636 kW/m^2 (7.5 ms) for 10 ms, 30 ms, and 50 ms spurt durations, respectively. Figures 6(*a*) and 6(*b*) also show that increasing the spurt duration increased the time when the surface remained at T_l (or $\bar{T}$) and decreased the rate of change of q''. Previous studies reported that T_l depends on spurt duration for nozzle-surface distances shorter than 25–30 mm but not for longer distances: T_l=−30°C for a 0.7 mm inner diameter nozzle and 50 mm nozzle-substrate distance [23,24]. Although there are differences in thermal sensors (location, type, and dimensions), spray system (nozzle geometries and nozzle-surface distance), and experimental conditions (relative humidity level) between the present and cited studies, our results are in agreement with observations for large distances: in the present study T_l=−33°C for each spurt duration, Fig. 6(*a*).

4.4 Spray and Tissue Phantom Fluid-Thermal Interactions. During the initial spray transient, when small and fast droplets wet the phantom surface, the greatest temperature drops and highest heat flux occurred because the temperature difference between the cryogenic liquid and warm substrate was at a maximum. If T is lower than the cryogen boiling temperature T_b, it is reasonable to assume that there is liquid cryogen on the surface. It follows that during most of the spray steady state, the surface was wet with a pool of liquid since $T<T_b$. For the 30 ms and 50 ms spurts, after spurt termination T departed from $\bar{T}$ ($t\approx$50 ms and 65 ms). For the 10 ms spurt, this departure occurred during the spray final transient state; a shorter spurt duration produced less accumulation of liquid cryogen during the spray steady state and, consequently, a surface—with a thinner pool—more sensitive to small changes in surface heat transfer.

During the final transient, droplets were smaller and faster but did not enhance the surface heat transfer. During this transient, there was an increase in the number flux followed by a decrease, Figs. 7(*a*)–7(*c*), while the mass flux, Figs. 7(*d*)–7(*f*), and kinetic energy flux, Figs. 7(*g*)–7(*i*), only decreased. Therefore, during the final transient, droplets had less energy to penetrate into the liquid pool enhancing heat transfer, and their accumulation appeared to be negligible due to a low mass flux. Furthermore, even if these droplets had impinged on a cryogen free surface, the temperature difference between liquid and substrate would have been minor resulting in small heat fluxes.

4.5 Temperature Estimation for Human Tissue. Figure 8 shows the estimated human tissue temperatures using the transformation introduced in Sec. 4.1 (Eq. (6)) and the experimental measurements presented in Fig. 6(*a*), i.e., the surface thermal responses of stratum corneum and epidermis substrates to CSC. Although CSC is never applied directly to the epidermis, it is relevant to calculate the epidermal thermal response to direct cooling to obtain an estimate of the lowest temperature boundary therein. $\bar{\theta}_{t,0.3}$=−22°C and $\bar{\theta}_{t,0.6}$=−2°C for $\bar{T}$=−33°C and an initial substrate temperature of 22.5°C. However, human tissue (skin) temperature is considerably higher, ≈32.5°C. Jia et al. [17] quantified the surface heat transfer during 50 ms (and 20 mm nozzle-substrate distance) CSC of substrates at different initial

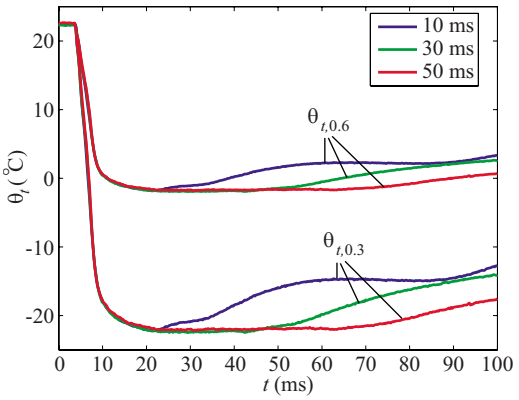

Fig. 8 Estimated human tissues surface thermal responses during CSC with 10 ms, 30 ms, and 50 ms spurts for tissues with 0.3 and 0.6 water contents

temperatures: 20°C, 40°C, and 80°C, for which the lowest substrate temperatures were, respectively, −40°C, −35°C and −30°C. A 20°C difference between initial temperatures resulted in a 5°C difference between the lowest temperatures. If the initial temperature was 32°C in our experiments, it is reasonable to assume that $\bar{T} \approx -30$°C, for which $\bar{\theta}_{t,0.3} \approx -19$°C and $\bar{\theta}_{t,0.6} \approx 0$°C. Since the stratum corneum is the most superficial layer of human skin with a thickness of 20 μm above the epidermal layer, epidermal temperatures during CSC are expected to be higher than 0°C even for larger spurt durations.

Phase change at subzero temperatures of biological components with a water composition was not considered in this study. The stratum corneum has a very low-water content since it is composed mainly of layers of dead cells. Our results show that the epoxy thermal response is closer to that of stratum corneum. If the phase change is present, then a tissue phantom with higher water content may be appropriate for considering the changes in thermal properties of tissue as a function of temperature, for example, TX-151 (≈65% water by volume).

5 Conclusions

Numerical modeling of epoxy and human tissues with 0.3 and 0.6 water contents (stratum corneum and epidermis, respectively) show that, subject to the same heat flux, their thermal response is qualitatively similar but the total temperature drops in tissues are about 81% and 43% less as compared to epoxy, respectively. Epoxy is a good thermal phantom to study low-water content tissues, such as the stratum corneum. A simple transformation can be used to map the temperature response of the epoxy to that of tissue. Using this transformation and experimental measurements on a tissue phantom, the lowest stratum corneum and epidermal temperatures in human tissue during CSC with commercial devices using 10 ms, 30 ms, and 50 ms spurts are estimated to be approximately −19°C and >0°C, respectively.

Despite the relative short spurt durations, cryogen delivery is mostly a steady state process with the initial and final transients mainly due to valve dynamics. Thermal transients are longer than fluid transients due to the low thermal diffusivity of human tissues; steady states are comparable in duration although there is an inherent thermal delay. During the initial spray transient, fast and small droplets (with respect to steady state values) induce large temperature drops and the highest heat flux since the temperature difference between cryogen and tissue phantom is greatest; during the spray steady state, surface temperature remains at its lowest value; during the final transient, droplets are fast and small again, although in this period their impact on the surface heat transfer is negligible due to the decreasing mass and kinetic energy fluxes and, in particular, reduced temperature differences between cryogen and tissue phantom. Steady state temperatures are the lowest surface temperatures experienced by the substrate, independent of spurt duration; hence, longer spurt durations result in larger exposures of the tissue to the same lower, steady state temperature as shorter spurts.

Acknowledgment

This work was supported by the following grants: AR 47551, AR 48458, and EB 2495 to J.S.N., and UCR Academic Senate Grant to G.A.

Nomenclature

A_γ = reference area of PDPA detection volume (m^2)
c = specific heat (J/(kg K))
D = droplet diameter (μm)
e_γ = unit vector
h = heat transfer coefficient (W/(m^2 K))
k = thermal conductivity (W/(m K))
L = characteristic length (m)
M = sample size or number of PDPA measurements
N = number of validated PDPA signals
n = normal unit vector
q'' = surface heat flux (W/m^2)
T = experimental temperature (°C)
t = time (s)
V = droplet velocity (m/s)
x = lateral coordinate (m)
y = depth coordinate (m)

Subscripts

b = boiling
e = epoxy
f = final
h = highest
I = total number of PDPA measurements
i = PDPA measurement
J = total number of temperature measurements
j = temperature measurement
l = lowest
o = initial
p = tissue phantom
s = phantom surface
t = tissue

Greek symbols

α = thermal diffusivity (m^2/s)
γ = particle trajectory angle
η = PDPA count correction factor
θ = numerical temperature (°C)
ξ = transformation coefficient
ρ = density (kg/m^3)
τ = measurement time (s)
φ = spray flux

References

[1] Nelson, J. S., Milner, T. E., Anvari, B., Tanenbaum, B. S., Kimel, S., Svaasand, L. O., and Jacques, S. L., 1995, "Dynamic Epidermal Cooling During Pulsed-Laser Treatment of Port-Wine Stain—A New Methodology With Preliminary Clinical Evaluation," Arch. Dermatol., **131**, pp. 695–700.

[2] Nelson, J. S., Milner, T. E., Anvari, B., Tanenbaum, S., Svaasand, L. O., and Kimel, S., 1996, "Dynamic Epidermal Cooling in Conjunction With Laser-Induced Photothermolysis of Port Wine Stain Blood Vessels," Lasers Surg. Med., **19**, pp. 224–229.

[3] Aguilar, G., Majaron, B., Pope, K., Svaasand, L. O., Lavernia, E. J., and Nelson, J. S., 2001, "Influence of Nozzle-To-Skin Distance in Cryogen Spray Cooling for Dermatologic Laser Surgery," Lasers Surg. Med., **28**, pp. 113–120.

[4] Karapetian, E., Aguilar, G., Kimel, S., Lavernia, E. J., and Nelson, J. S., 2003, "Effects of Mass Flow Rate and Droplet Velocity on Surface Heat Flux During Cryogen Spray Cooling," Phys. Med. Biol., **48**, pp. N1–N6.

[5] Pikkula, B. M., Tunnell, J. W., Chang, D. W., and Anvari, B., 2004, "Effects of Droplet Velocity, Diameter, and Film Height on Heat Removal During Cryogen Spray Cooling," Ann. Biomed. Eng., **32**, pp. 1131–1140.

[6] Franco, W., Liu, J., Wang, G. X., Nelson, J. S., and Aguilar, G., 2005, "Radial and Temporal Variations in Surface Heat Transfer During Cryogen Spray Cooling," Phys. Med. Biol., **50**, pp. 387–397.

[7] Franco, W., Liu, J., Romero-Méndez, R., Jia, W., Nelson, J. S., and Aguilar, G., 2007, "Extent of Lateral Epidermal Protection Afforded by a Cryogen Spray Against Laser Irradiation," Lasers Surg. Med., **39**, pp. 414–421.

[8] Hsieh, S. S., and Tsai, H. H., 2006, "Thermal and Flow Measurements of Continuous Cryogenic Spray Cooling," Arch. Dermatol. Res., **298**, pp. 82–95.

[9] Jia, W., Choi, B., Franco, W., Lotfi, J., Aguilar, G., and Nelson, J. S., 2007, "Treatment of Cutaneous Vascular Lesions Using Multiple- Intermittent Cryogen Spurts and Two-Wavelength Laser Pulses: Numerical and Animal Studies," Lasers Surg. Med., **39**, pp. 494–503.

[10] Aguilar, G., Diaz, S. H., Lavernia, E. J., and Nelson, J. S., 2002, "Cryogen Spray Cooling Efficiency: Improvement of Port Wine Stain Laser Therapy Through Muttiple-Intermittent Cryogen Spurts and Laser Pulses," Lasers Surg. Med., **31**, pp. 27–35.

[11] Anvari, B., Tanenbaum, B. S., Hoffman, W., Said, S., Milner, T. E., Liaw, L. H. L., and Nelson, J. S., 1997, "Nd:YAG Laser Irradiation in Conjunction With Cryogen Spray Cooling Induces Deep and Spatially Selective Photocoagulation in Animal Models," Phys. Med. Biol., **42**, pp. 265–282.

[12] Tate, R. W., 1982, Some Problems Associated With The Accurate Representation Of Droplet Size Distributions, Proceedings of the 2nd Iclass.

[13] Jia, W., Aguilar, G., Verkruysse, W., Franco, W., and Nelson, J. S., 2006,

"Improvement of Port Wine Stain Laser Therapy by Skin Preheating Prior to Cryogen Spray Cooling: A Numerical Simulation," Lasers Surg. Med., **38**, pp. 155–162.
[14] Majaron, B., Kimel, S., Verkryusse, W., Aguilar, G., Pope, K., Svaasand, L. O., Lavernia, E. J., and Nelson, J. S., 2001, "Cryogen Spray Cooling in Laser Dermatology: Effects of Ambient Humidity and Frost Formation," Lasers Surg. Med., **28**, pp. 469–476.
[15] Franco, W., Liu, J., and Aguilar, G., 2005, "Interaction of Cryogen Spray With Human Skin Under Vacuum Pressures," in *Fluid Structure Interaction and Moving Boundary Problems*, S. Chakrabari, S. Hernandez, and C. A. Brebia, eds., Wessex Institute of Technology, Southampton, UK, pp. 153–162.
[16] Roisman, I. V., and Tropea, C., 2001, "Flux Measurements in Sprays Using Phase Doppler Techniques," Atomization Sprays, **11**, pp. 667–669.
[17] Jia, W., Aguilar, G., Wang, G. X., and Nelson, J. S., 2004, "Heat-Transfer Dynamics During Cryogen Spray Cooling of Substrate at Different Initial Temperatures," Phys. Med. Biol., **49**, pp. 5295–5308.
[18] Incropera, F. P., and Dewitt, D. P., 1996, *Fudamentals of Heat and Mass Transfer*, Wiley, New York.
[19] Beck, J. V., Blackwell, B., and St. Clair, C. R., Jr., 1985, *Inverse Heat Conduction: III Posed Problems*, Wiley, New York.
[20] Jacques, S. L., Nelson, J. S., Wright, W. H., and Milner, T. E., 1993, "Pulsed Photothermal Radiometry of Port-Wine-Stain Lesions," Appl. Opt., **32**, pp. 2439–2446.
[21] Caspers, P. J., Lucassen, G. W., Bruining, H. A., and Puppels, G. J., 2000, "Automated Depth-Scanning Confocal Raman Microspectrometer for Rapid In Vivo Determination of Water Concentration Profiles in Human Skin," J. Raman Spectrosc., **31**, pp. 813–818.
[22] Aguilar, G., Majaron, B., Karapetian, E., Lavernia, E. J., and Nelson, J. S., 2003, "Experimental Study of Cryogen Spray Properties for Application in Dermatologic Laser Surgery," IEEE Trans. Biomed. Eng., **50**, pp. 863–869.
[23] Aguilar, G., Wang, G. X., and Nelson, J. S., 2003, "Dynamic Behavior of Cryogen Spray Cooling: Effects of Spurt Duration and Spray Distance," Lasers Surg. Med., **32**, pp. 152–159.
[24] Aguilar, G., Wang, G. X., and Nelson, J. S., 2003, "Effect of Spurt Duration on the Heat Transfer Dynamics During Cryogen Spray Cooling," Phys. Med. Biol., **48**, pp. 2169–2181.
[25] Tunnell, J. W., Torres, J. H., and Anvari, B., 2002, "Methodology for Estimation of Time-Dependent Surface Heat Flux Due to Cryogen Spray Cooling," Ann. Biomed. Eng., **30**, pp. 19–33.